Simulation of Grating-Compressor Misalignment Tolerances and Mitigation Strategies for Chirped-Pulse–Amplification Systems of Varying Bandwidth and Beam Size

Introduction

For more than 30 years, chirped-pulse amplification (CPA) has made it possible to amplify picosecond and femtosecond pulses to high energy by circumventing the damage threshold limitations of direct amplification via pulse stretching and compression.[1] CPA has found wide application in a variety of laser amplifier technologies including fiber, solid-state, gas, excimer, mixed-bulk glasses, and optical parametric amplifiers. These technologies are integrated into CPA systems ranging in peak powers from gigawatt (GW) (Ref. 2) to petawatt (PW) (Ref. 3). The peak power of a CPA system is constrained to some degree by the choice of amplifier technology. The pulse duration is limited by the bandwidth of the medium, and the size/geometry of the medium can impose limits on energy scaling.

Diffraction gratings are by far the most common elements used to stretch and compress pulses because of their substantial angular dispersion, where pulse-stretching factors typically range from 1000 to 100,000. These gratings typically function in pairs, where the first diffraction grating spreads the bandwidth in space and the second grating cancels the angular dispersion of the first, consequently introducing group-delay dispersion (GDD) from the wavelength-dependent variation of path length. If the second grating is not perfectly parallel to the first grating, the residual angular dispersion can cause errors in pulse compression and focusability, impacting the spatiotemporal shape of the pulse and reducing the overall focused intensity.

The three primary effects of angular dispersion are increased beam divergence affecting the minimum focused spot size, tilt of the pulse front, and errors in chirp or spectral dispersion affecting the pulse duration.[4] These and other more-subtle effects complicate the calculation of grating-alignment tolerances for many systems,[5–7] where individualized time-intensive simulations are required to determine alignment sensitivity for a particular CPA system. Depending on system specifications and desired performance, grating-alignment tolerances may necessitate the use of high-performance or specialized mounting hardware for stability and alignment precision. An understanding of how grating-alignment tolerances scale with CPA parameters such as bandwidth and beam size can provide early determination of whether intensive simulation or specialized mounting hardware may be required for a particular system, which may affect project budget, resources, or time line.

In this work, compressor grating-alignment sensitivity is compared for CPA systems ranging in Fourier transform–limited (FTL) pulse duration from 10 fs to 1 ps and for beam sizes from 10 mm to 300 mm. Grating-tilt–alignment tolerances are defined and simulated for varying compressor groove density from 900 to 2000 gr/mm and for all possible incident angles. To our knowledge, this is the first time that grating-alignment tolerances have been specified plainly over such a broad range of parameters. These tolerances serve as guidelines to indicate which combinations of bandwidth, beam size, groove density, and incident angle are most sensitive to misalignment. Techniques for compensating grating-misalignment errors are simulated, and limitations are identified for broad bandwidth, affecting intensity and temporal contrast.

Effects of Grating Misalignment on Pulse Compression

Each grating in a stretcher or compressor must be aligned in three dimensions: tilt, tip, and in-plane rotation (IPR) (Fig. 155.19). Generally, the incident and diffracted rays have a component in the plane of diffraction and the plane of reflection. In a perfectly aligned compressor, where grating pairs have parallel surfaces and grooves, the incident and diffracted rays lie solely in the x–z plane with no component in the reflection plane (y–z plane). Grating-tilt misalignment changes the incident/diffracted angles, but the plane of diffraction remains coplanar with the x–z plane. Tilt error of one grating in a pair causes angular dispersion in the x–z plane at the compressor output. Tip and IPR misalignment produces a nonzero component in the reflection plane and effectively rotates the plane of diffraction with respect to the plane of incidence. Rotation of the diffraction plane creates a component of residual angular dispersion, which is perpendicular to the x–z plane. Angular dispersion produced by any misalignments has a temporal and spatial effect on the compressor output.

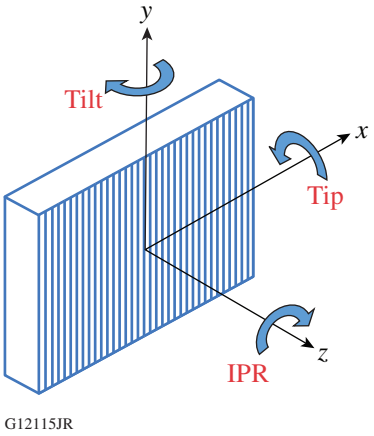

Figure 155.19
Definition of grating-alignment parameters and axes. IPR: in-plane rotation.

In the time domain, angular dispersion from a misaligned grating compressor causes a tilt of the pulse front or an inhomogeneous wave so that one edge of the beam is delayed with respect to the other.[8] If the beam is sampled locally, the pulse duration will appear short; however, the spatially integrated pulse duration and the duration of illumination at the focal plane are much longer because of the pulse-front delay.[6] In addition, grating misalignment changes the path length of each wavelength component so that the total system GDD is no longer minimized. This GDD mismatch can also vary spatially across the beam, degrading the spatiotemporal quality of the compressed pulse.

In the spatial domain, residual angular dispersion from a misaligned grating pair affects focusability because of increasing beam divergence. This causes an elongation of the minimum spot size in the direction of the angular dispersion error. Tilt error exhibits spot elongation purely in the horizontal (x–z) plane, while tip and IPR add a vertical elongation from slight rotation of the diffraction plane out of the horizontal plane.

Other effects to consider are finite beam size, lateral frequency shift, higher-order dispersion, and grating astigmatism.[5,9] Many models neglect the effect of beam divergence or free-space diffraction, but these effects are not trivial for large bandwidths, small waists, and beam collimation errors. Diverging rays from free-space diffraction take a slightly different path through a grating pair and can contribute to spatial variations in chirp across the beam. For large bandwidth, the beam waist, and therefore the divergence angle, is wavelength dependent, further complicating calculation of these effects.

For the case of narrow bandwidth and for a compressor beam size that is much larger than the spatial extent of the pulse duration, there is a convenient, simple analytical expression that describes broadening of the pulse duration at the focal plane resulting from pulse-front tilt (PFT):[8,10]

$$\Delta\tau = D\frac{N\lambda_0}{c}\frac{\tan(\beta_0)}{\cos(\alpha)}\epsilon_x, \tag{1}$$

$$\tau = \sqrt{\tau_0^2 + (u\Delta\tau)^2}\,. \tag{2}$$

The equation for pulse duration increase $\Delta\tau$ is linear with compressor beam size D and grating tilt error ϵ_x, where N is the grating groove density, α is the incident angle, and β_0 is the diffracted angle for the center wavelength λ_0. The total pulse duration at focus τ is the root square sum of the FTL pulse duration τ_0 and PFT broadening $\Delta\tau$, where u is the conversion factor from $1/e^2$ to full-width-at-half-maximum (FWHM) duration.

Simulations in *FRED*, a beam propagation software by Photon Engineering[11] (solid lines in Fig. 155.20), closely match the analytical expression [Eq. (2)] for PFT with a 300-mm

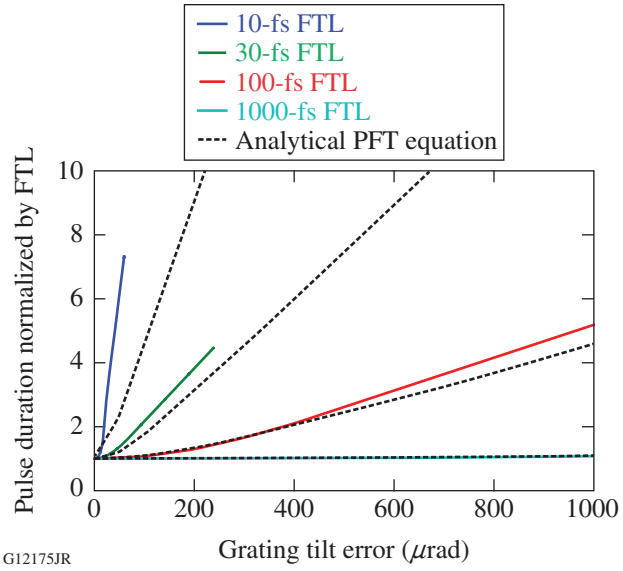

Figure 155.20
The solid lines are simulations of the pulse-duration increase because of grating tilt for several different Fourier transform–limited (FTL) pulse durations (i.e., bandwidth) in a 300-mm-diam compressor beam. The dashed lines follow the analytical solution [Eq. (1)] for pulse-duration increase caused by pulse-front tilt (PFT), valid for narrow bandwidth and cases where beam size is much larger than the spatial extent of the pulse duration.[8] Simulations here are for 900-nm center wavelength, 1285-gr/mm grating groove density, 51° incident angle, and 300-mm compressor beam diameter.

compressor beam size in the case of a 1000-fs pulse duration. For larger bandwidth (i.e., shorter FTL pulse duration) and grating-tilt error, however, the accuracy of Eq. (2) degrades. Large-bandwidth compressors must also consider the effect of spectral chirp and other higher-order effects that are wavelength dependent.

The combination of multiple space–time effects make calculation problematic, and in many cases complex simulations utilizing ray-tracing or beam propagation software are required. Calculations are more accurate when modeling software takes into account relative contributions from multiple space–time effects as well as free-space diffraction.[5] One goal of this work, discussed in **Scaling of Compressor Alignment Tolerances for CPA Systems with Bandwidth, Energy, and Compressor Geometry** (p. 146), is to define the limits where a higher level of analysis is required.

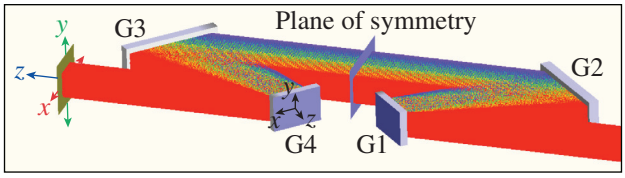

Figure 155.21
FRED model of a four-grating (G1–G4) pulse compressor. Optionally, a single grating pair can be used by placing a vertical roof mirror at the plane of symmetry.

Simulation of Grating Compressor Sensitivity for a 0.5-PW OPCPA System

To illustrate the relative alignment sensitivity between tilt, tip, and IPR for a four-grating compressor (Fig. 155.21), a *FRED–MATLAB* model[12] is used to simulate alignment sensitivity for the 0.5-PW MTW OPAL (Multi-Terawatt optical parametric amplifier line), 15-fs optical parametric CPA (OPCPA) system.[13] Originally this simulation code was developed for compressor simulations on OMEGA EP.[14]

The compressor model (Fig. 155.21) propagates Gaussian beamlets through gratings and other optics, recording the spatial (x,y) and spectral (ω) amplitude and phase in a 3-D complex matrix. Next, a *MATLAB*[15] postprocessor computes the integrated near-field and far-field beam profiles and pulse durations from this 3-D matrix (Fig. 155.22). The previous steps are repeated for a range of grating misalignments. Tolerances for pulse duration and/or focused spot size can be determined from alignment sensitivity plots (Fig. 155.23).

The pulse duration increases most dramatically with tilt error from the second and third gratings (Fig. 155.23). Because the beam and spectrum are spread across this grating, there is a larger amount of induced GDD error with misalignment compared to the first (and fourth) grating. Assuming that misalignments occur slowly over time (i.e., no significant high-frequency pointing errors from vibration), the grating distance can be adjusted to compensate for some of the extra GDD error so that the alignment sensitivity of the second (and third) grating nearly matches the first (and fourth) grating. Compensation of grating misalignment will be discussed in **Mitigation Strategies for the Effects of Grating Misalignment in Pulse Compressors and Their Limitations** (p. 150). The alignment

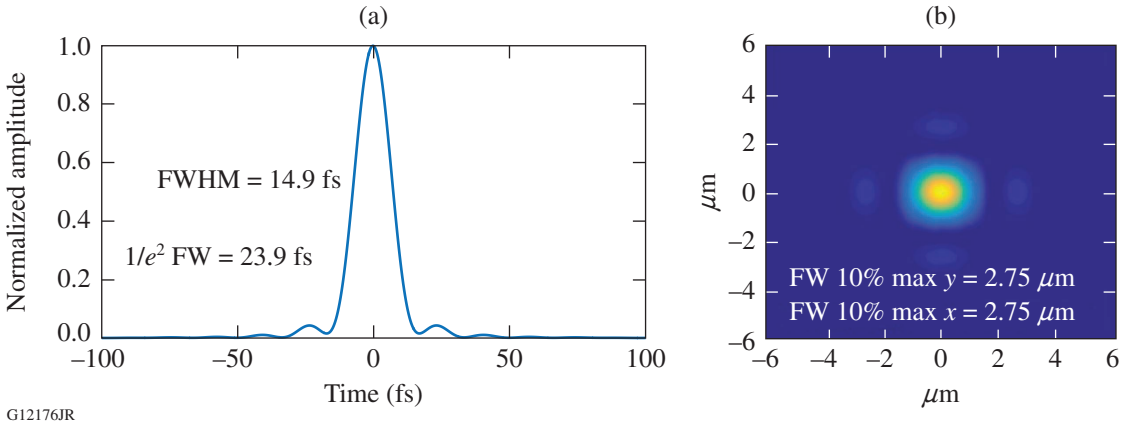

Figure 155.22
Results of a simulation using the *FRED* beam-propagation model and *MATLAB* postprocessor: (a) the spatially integrated far-field pulse duration and (b) the temporally integrated focused spot size.

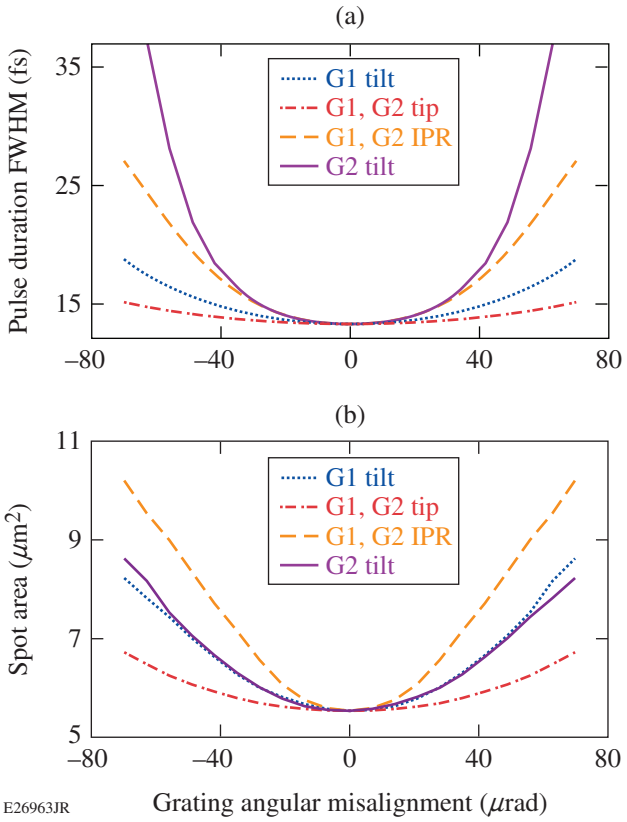

Figure 155.23
Simulated far-field (a) pulse duration FWHM and (b) spot area full-width (FW) 10% of max for the 0.5-PW Multi-Terawatt optical parametric amplifier line (MTW OPAL) optical parametric chirped-pulse–amplification (OPCPA) system at LLE.[13] Only one type of error (tilt, tip, or IPR) is applied at a time to each grating, while the grating separation remains fixed. MTW OPAL output specifications: 15-fs pulses centered at 900 nm, 90-mm compressor beam diameter, 50° grating incident angle, and 1285 gr/mm.

sensitivity of both tip and the IPR is similar in magnitude to tilt but their relative sensitivity is strongly dependent on the compressor parameters and will be presented in greater detail.

Scaling of Compressor Alignment Tolerances for CPA Systems with Bandwidth, Energy, and Compressor Geometry

1. Bandwidth and Energy Scaling of Grating-Tilt Tolerances

CPA systems can be generally classified in terms of peak power. While grating-alignment sensitivity is not directly influenced by peak power, energy and pulse duration can be transformed into parameters that directly affect the grating-alignment sensitivity.

The FTL pulse duration is inversely proportional to the bandwidth of a CPA system, where increasing bandwidth expands the spread of angular dispersion, increasing pulse duration and focused spot size. The compressor beam size is another parameter that is known to have a direct effect on grating-alignment sensitivity.[8] The beam size in a compressor is regulated by the laser-induced damage threshold (0.2 to 0.3 J/cm^2 for gold[16] and 1 to 2 J/cm^2 for dielectric[17]) and therefore can be loosely transformed into energy.

The parameters of bandwidth and beam size provide a framework with which to describe grating-alignment sensitivity and tolerances. Common CPA system amplifier technologies are mapped into this space (Fig. 155.24) in order to approximate alignment tolerances generally for these classes of systems [Fig. 155.25(a)].

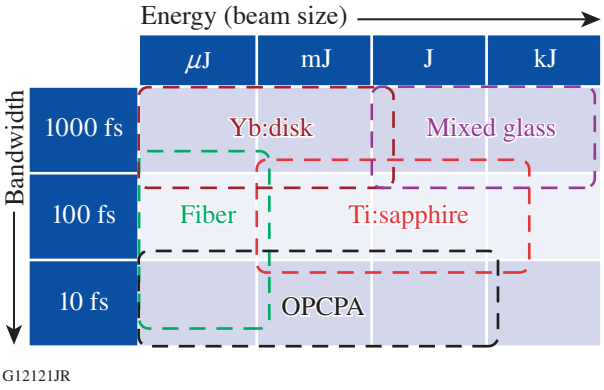

Figure 155.24
Framework for mapping several mainstream chirped-pulse–amplification (CPA) technologies in terms of bandwidth and compressor beam size.

The *FRED–MATLAB* model described earlier was adapted for altering beam sizes and pulse bandwidths in order to simulate how grating-tilt–alignment tolerances scale with compressor beam size and transform-limited pulse duration. Other compressor parameters such as the 900-nm center wavelength, 50° grating incident angle, groove density of 1285 mm^{-1}, and 1.2-m grating separation (GDD of ~6 × 10^6 fs^2) remain constant. The compressor beam size is varied from 10 mm to 300 mm and the FTL pulse duration is varied from 10 fs to 1 ps [Fig. 155.25(b)]. While only tilt tolerances are specified from this study, relative tip and IPR tolerances can be predicted and will be discussed in **Mitigation Strategies for the Effects of Grating Misalignment in Pulse Compressors and Their Limitations** (p. 150).

A somewhat arbitrary tolerance is defined for a $\sqrt{2}$ factor drop in intensity compared to a FTL duration and diffraction-limited (DL) spot area:

(a)

Beam size →

Bandwidth ↓ / Tilt tolerance (μrad)	10 mm	50 mm	100 mm	300 mm
1000 fs	24k	18k	6k	1.9k
100 fs	1.3k	848	491	179
30 fs	89	74	74	44
10 fs	22	21	20	13

G12197JR

(b)

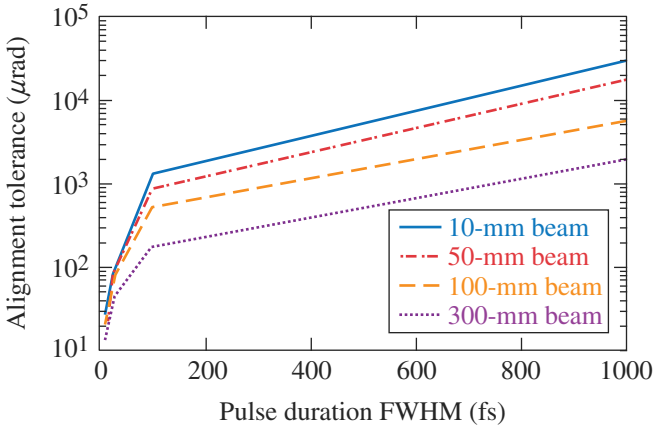

Figure 155.25

(a) Second grating-tilt–alignment tolerances for FTL pulse duration and compressor beam size (matching Fig. 155.24); the light-blue shaded region shows tilt-alignment tolerances <500 μrad. (b) Plot of the same tilt-alignment tolerances with pulse duration for multiple beam sizes in a four-grating compressor with a 900-nm center wavelength and 1285-gr/mm gratings separated by 1.2 m. Tolerances are based on an intensity reduction by a factor of $\sqrt{2}$ as a result of space–time pulse aberrations.

$$I_{\text{tolerance}} = \frac{I_{\max}}{\sqrt{2}}. \tag{3}$$

Since intensity is inversely proportional to pulse duration and spot area, the tolerance is reached when the normalized product of pulse duration and spot area is equal to $\sqrt{2}$:

$$\frac{\tau}{\tau_{\text{FTL}}} \cdot \frac{A}{A_{\text{DL}}} = \sqrt{2}. \tag{4}$$

This tolerance definition takes into account increases in both pulse duration and spot size for applications where intensity on target is critical.

Since grating-alignment tolerances are highly dependent on bandwidth and compressor beam size, tolerances can be specified in this framework and broadly applied to various CPA system classes (Figs. 155.24 and 155.25). Tolerance estimations provide useful information about feasibility and effort level or resources required for compressor design and construction.

2. Grating Groove Density and Incident Angle Scaling of Grating-Tilt Tolerances

In addition to bandwidth and compressor beam size, grating-alignment tolerances will depend on other parameters, such as grating groove density, grating separation, wavelength, incident/diffracted angles, and application requirements (e.g., pulse duration, spot size, or intensity).

After selecting a tolerance from Fig. 155.25 for a particular bandwidth and beam size, it is important to determine how this tolerance scales with groove density and incident angle for a particular compressor geometry. When designing a compressor, there are various suitable combinations of incident/diffracted angle and grating groove densities, which can be selected based on desired dispersion profiles, size constraints, alignment sensitivity, diffraction efficiency, etc. Incident and diffracted angle ranges for each groove density option are limited by the physical size of beams (including the spread of the bandwidth in space), real diffraction angles from the grating equation, grating-size constraints, and grating separation (i.e., magnitude of GDD required for compression of the stretched pulse).

For example, the angle between the incident and diffracted beams near Littrow is limited for real beams by

$$\alpha > \beta_{\text{r}} + \sin^{-1}\left[\frac{D\cos\beta_{\text{r}}}{G}\right] \quad \text{for } \alpha > \theta_{\text{Littrow}}, \tag{5}$$

$$\alpha < \beta_{\text{b}} - \sin^{-1}\left[\frac{D\cos\beta_{\text{b}}}{G}\right] \quad \text{for } \alpha < \theta_{\text{Littrow}}, \tag{6}$$

where α is the incident angle, $\beta_{\text{r/b}}$ is the diffracted angle for the wavelengths at the red and blue edges of the bandwidth, D is the compressor $1/e^2$ beam diameter, G is the perpendicular grating separation, and θ_{Littrow} is the angle at which the dif-

fracted angle for the center wavelength and the incident angle are equal.

Figure 155.26(a) shows all possible diffraction and incident angles for several common groove densities based on a 100-mm compressor beam size with a 180-nm "full-width" bandwidth (30-fs FTL), assuming a GDD of 6×10^6 fs^2 and a maximum grating width of 600 mm.

Grating-tilt tolerances [defined by Eq. (4)] were simulated for a four-grating compressor using the *FRED–MATLAB* model for 23 combinations of grating groove densities and incident angles [spread over the ranges shown in Fig. 155.26(a)] for a fixed bandwidth of 30-fs FTL and 100-mm compressor beam size. The simulated tilt tolerances for the second grating [solid lines in Fig. 155.26(b)] are compared to estimated tolerances based on Eq. (1) for PFT [dashed lines in Fig. 155.26(b)]. The differences between the PFT approximation tolerances and the simulated tolerances in Fig. 155.26(b) are primarily caused by the temporal chirp effect from the 30-fs FTL bandwidth since the PFT approximation does not include the local pulse broadening from GDD, nor does it explicitly include the far-field intensity reduction from the elongated focal spot. The breakdown of the PFT approximation with increasing tilt error and bandwidth is shown earlier in Fig. 155.20.

Since the tolerances are defined by Eq. (4), the ratio of the normalized pulse duration to the normalized spot area [Fig. 155.26(c)] reveals how relative contributions from temporal or spatial aberrations impact the intensity tolerance [Eq. (3)]. In Fig. 155.26(c) the pulse-to-area ratio is close to $\sqrt{2}$ for small incident angles, where elongation of the focal spot is nominal. For larger angles of incidence, the relative contribution of the focal-spot area to the tolerance is greater, indicating a larger

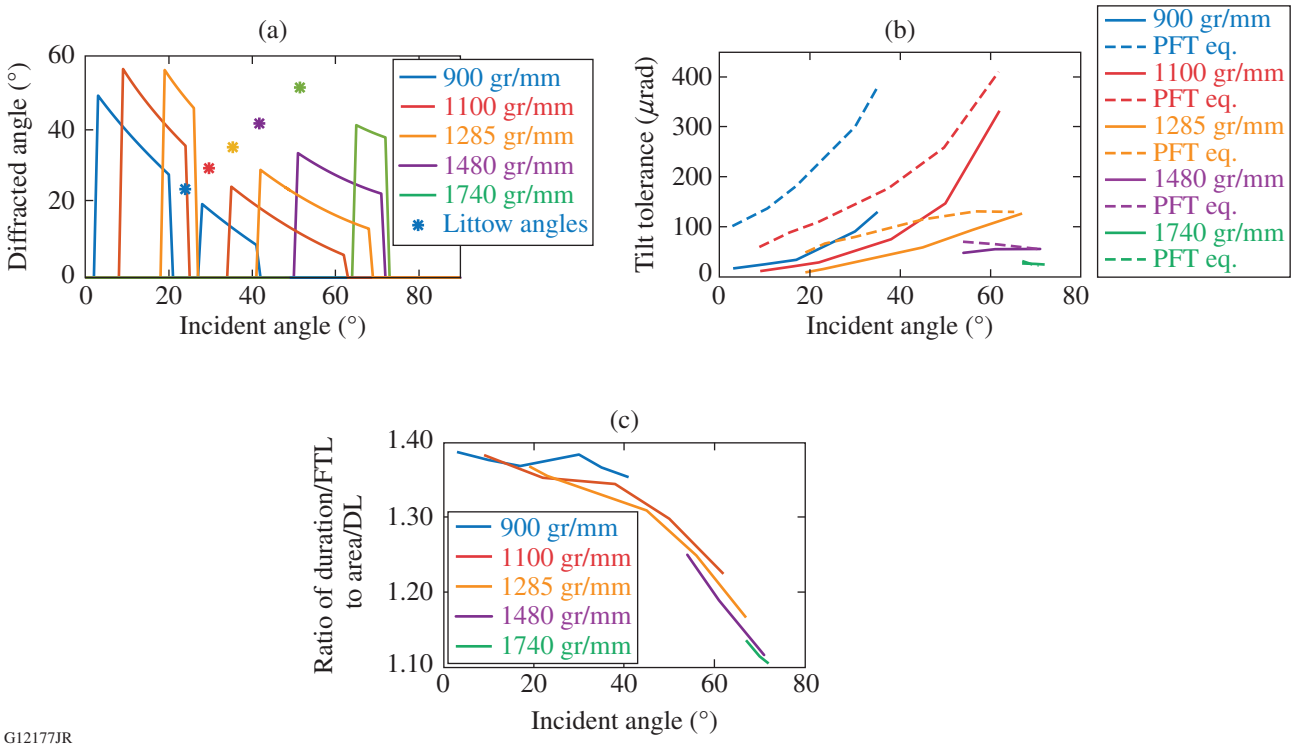

Figure 155.26

(a) All possible combinations of diffracted and incident angles are shown for several common grating groove densities, limited by beam size, spectrum, and grating aperture. Diffracted angles are set to zero for all nonphysical combinations near the Littrow angles (also assuming a fixed group delay dispersion of 6×10^6 fs^2) indicated by asterisks. Additionally, large incident angles and diffracted angles are set to zero in cases where beam widths on gratings are >600 mm. (b) Twenty-three tilt-tolerance simulations were performed (solid lines) to analyze grating-tilt–tolerance trends in the range of possible incident angles and groove densities [shown in (a)]. The dashed lines show the tilt tolerance using only the pulse-front–tilt estimation [Eqs. (1) and (2)]. (c) The ratio of pulse duration normalized by the FTL and spot area normalized by the diffraction limit (DL), assuming perfect compressor alignment, is shown for varying incident angle and grating groove density to reveal the relative impact of temporal and spatial aberrations on the intensity tolerance [Eqs. (3) and (4)].

contribution from angular dispersion. This is consistent with further analysis that showed larger temporal shear (group delay) across the near-field beam with incident angle for tilt errors equal to the tolerance limit, and smaller contributions from local GDD. The local GDD was calculated by fitting the spectral phase at the beam center to a polynomial and extracting the second-order coefficient. The pulse-to-area ratio in Fig. 155.26(c) is closer to one for the largest incident angles and grating groove densities, indicating nearly equal contributions of pulse duration and area to the intensity tolerance.

To illustrate tolerance scaling with a high resolution over the full parameter space, Eqs. (1) and (2) were employed to estimate tilt tolerances for groove densities ranging from 800 to 2000 gr/mm and for all possible incident angles [Fig. 155.27(a)]. Figure 155.27(b) shows the simulated data points from Fig. 155.26(b), which have been linearly extrapolated over the entire parameter space.

The white regions in Fig. 155.27 represent nonphysical solutions from either too close a proximity to Littrow [dashed line in Fig. 155.27(a)] or beams that were too large (the grating size was somewhat arbitrarily limited to 600 mm). The dashed line highlighting the Littrow angle separates two types of compressor geometry, where the incident angle is larger than diffracted (right) and vice versa (left). In general, tolerances are much tighter for larger groove densities and smaller incident angles, where compressors with incident angles smaller than diffracted angles are most sensitive to misalignment.

Figures 155.26(b) and 155.27 show how the tilt tolerance for the second and third gratings in a four-grating compressor over a range of incident angles and groove densities are much tighter for a modest 30-fs FTL bandwidth compared to the PFT approximation for narrow bandwidth. The true tilt tolerances can be up to a factor of 4 smaller compared to the approximations from Eq. (1) at low incident angle and groove densities [left side of Fig. 155.26(b) and left island in Fig. 155.27(b)] caused by a strong chirp effect [Fig. 155.26(c)], while tolerances for large incident angle and groove density are nearly equal with the PFT approximation [right side of Fig. 155.26(b) and top of the right island in Fig. 155.27(b)]. Since the tolerances defined by the PFT equation consider only the first-order variation of group delay with beam height, but are closely matching the simulation for large incident angle and groove density, the contribution of PFT dominates in this regime [Fig. 155.26(c)].

In Figs. 155.26(b) (dashed lines) and 155.27(a), the PFT approximation shows an inflection point where the tolerance

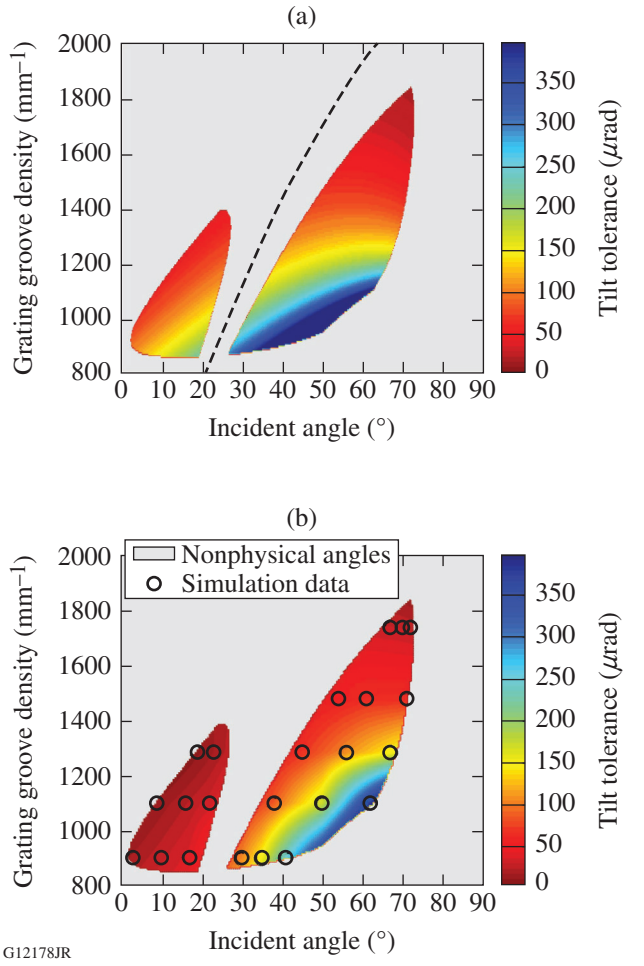

Figure 155.27
Variation in the second grating's tilt tolerance with groove density and incident angle for a 30-fs FTL bandwidth and 100-mm compressor beam diameter. Gray areas represent nonphysical combinations of incident angle and groove density [the same assumptions as in Fig. 155.26(a)]. (a) This intensity map was created from Eqs. (1) and (2), considering only the effect of PFT. Two islands of operation are identified for incident angles greater and less than the Littrow angle (dashed line). (b) Simulated data from Fig. 155.26(b) are extrapolated for all incident angles and groove densities, where circles show simulated data points.

is increasing with incident angle for groove density less than ~1500 gr/mm, but for larger groove density, the tolerance is decreasing with incident angle. A similar inflection point manifests in the simulation data [Figs. 155.26(b) and 155.27(b) right island] since the PFT and spot area contributions are stronger for larger incident angles in the right island [Fig. 155.26(c)]. Also note the slope of the tilt tolerance contour lines in Fig. 155.27(b) for groove density <1500 gr/mm is increased compared to Fig. 155.27(a) because of the strength of chirp effects on the pulse duration [Fig. 155.26(c)] for smaller incident angles, pulling down the tolerances in the left island significantly.

As a result of the complexity of effects influencing both the pulse duration and spot size, simulation is critical for larger bandwidth systems to accurately predict alignment tolerances. However, the trends shown in these generalized simulations can aid in estimating grating-alignment tolerances simply over a broad range of parameters suitable for most CPA systems and compressor designs.

Mitigation Strategies for the Effects of Grating Misalignment in Pulse Compressors and Their Limitations

1. Sources of Alignment Error

Sources of alignment error in grating compressors must be identified in order to assess strategies for mitigating pulse duration and spot-size errors. User error can improve with knowledge and practice of alignment techniques. One common alignment technique[18] reflects an alignment beam at normal incidence from the first grating to remove tip errors; the grating is then rotated to Littrow angle to remove IPR errors. Next, the first grating is rotated to its designated angle of incidence and the process is repeated for all consecutive gratings. The accuracy of these alignment techniques is typically limited by hardware. For example, a grating-tilt axis that is not orthogonal to the x–z reference plane of the compressor, or motion of this axis (i.e., wobble) in a rotation stage, typically in the range of 10 to 50 μrad, produces tip and IPR errors when rotating each grating from normal to Littrow during alignment. Using two wavelengths and two Littrow angles that are close together can minimize the wobble error during alignment.[19] Furthermore, the tolerances or resolution of tools and diagnostics such as corner cubes, irises, or cameras may add to alignment error.

Most alignment error stems from the grating mount and associated hardware performance since thermal drift and vibrations can cause slow or fast changes in the alignment. In the most-sensitive compressors, fluctuations resulting from vibration could cause pulse-duration or focal-spot instability. When non-gimbal mounts are used for grating alignment, there is cross coupling between adjustment axes, which complicates alignment.

2. Alignment Error Mitigation Strategies and Limitations

Pulse distortion as a result of grating-tilt errors is caused by a combination of pulse-front tilt and mismatched residual chirp. If these tilt errors are produced on a slow time scale, adjusting the grating separation can compensate for some of the residual chirp to mitigate the effect of pulse broadening. Additionally, finer control or arbitrary shaping of the spectral phase (applied uniformly across the beam) can further shorten the pulse duration to the limit of pulse-front tilt and other higher-order effects [Fig. 155.28(a)]. This is demonstrated via simulation by adjusting the grating separation after misalignment until the pulse duration is minimized. Arbitrary shaping of the dispersion by an acousto-optic programmable dispersive filter (AOPDF)[20] is

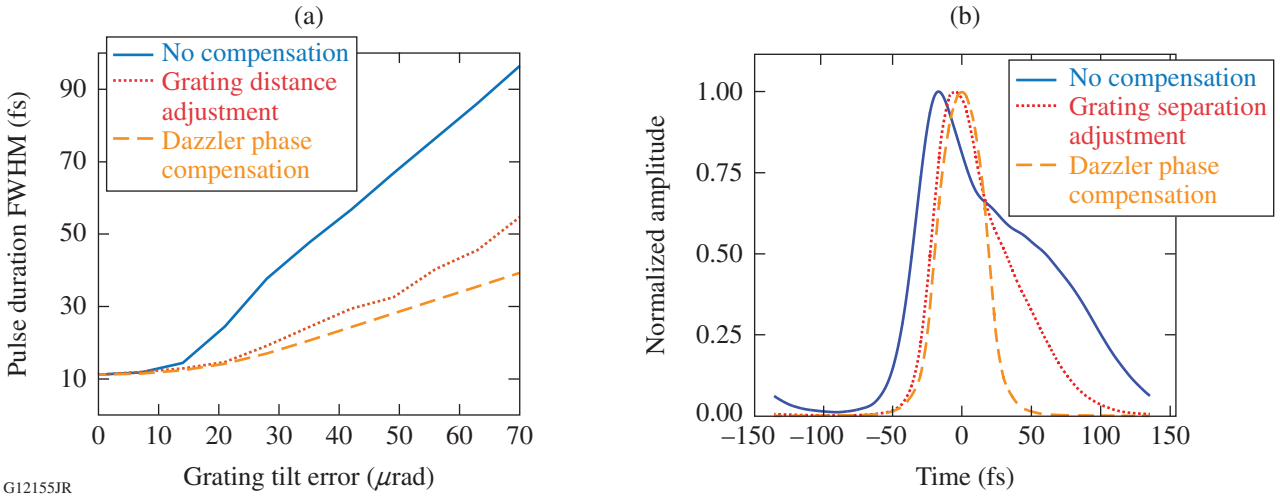

Figure 155.28

Techniques for compensation of residual chirp in the spatially integrated far-field (FF) pulse duration as a result of grating-tilt misalignment of the second grating. (a) Pulse duration is increased from 10-fs FTL with grating-tilt error; (b) shape and duration of the temporal pulse after 70 μrad of second-grating-tilt error are minimized by grating separation optimization and arbitrary shaping of the spectral phase (applied uniformly across the beam spatial profile). Arbitrary shaping of the spectral phase can be accomplished with an acousto-optic programmable dispersive filter (AOPDF), such as a Dazzler by Fastlite.[20]

simulated by subtracting the spatially averaged residual spectral phase across the beam. The asymmetric pulse shapes seen in Fig. 155.28(b) signify the presence of third-order dispersion, which is considerably improved in the case of AOPDF-like control of the spectral phase.

Grating tip and IPR alignment scale in sensitivity similar to tilt alignment with bandwidth and beam size. However, the relative sensitivity between tip and IPR is heavily dependent on the diffracted angle of the center wavelength. The vertical component of angular dispersion induced by tip error in a grating compressor can be represented to the first order by

$$\frac{\partial \phi_y}{\partial \lambda} = \left| 2\epsilon_y N \tan\left(\beta_0\right) \right|, \tag{7}$$

where N is the grating groove density and β_0 is the diffracted angle for the center wavelength.[6] Similarly, angular dispersion from IPR error (ϵ_z) in the vertical plane follows

$$\left| \frac{\partial \phi_y}{\partial \lambda} \right| = \left| 2\epsilon_z N \right|. \tag{8}$$

For systems with a narrow bandwidth, setting Eqs. (1) and (2) equal shows the ratio of IPR to tip sensitivity:

$$\left| \frac{\epsilon_z}{\epsilon_y} \right| = \left| \tan\left(\beta_0\right) \right|. \tag{9}$$

For diffracted angles of less than 45°, such as the MTW OPAL example in Fig. 155.23, where $\beta_0 = 22.55°$, IPR is more sensitive than the tip. Conversely, the compressed pulse duration increases more quickly with tip error for diffracted angles greater than 45°.

The relation in Eq. (9) indicates that a prescribed amount of tip can compensate for IPR error and vice versa.[7] *FRED–MATLAB* simulations searched for the amount of tip needed to optimize the pulse duration after an array of IPR errors and found good agreement with Eq. (9) for a couple of extreme combinations of bandwidth and beam-size variation (Fig. 155.29).

For an ultrabroadband 10-fs FTL pulse, IPR errors up to 200 μrad can be compensated with tip at the expense of a <25% increase in pulse duration from FTL [Fig. 155.30(a)]. This increase is <15% for a 20-fs pulse and <4% for a 30-fs pulse. The pulse shapes in Fig. 155.30(b) have a shape similar to a sinc-squared function as a result of the 20th-order super-Gaussian shape of the spectrum, typical for many ultrabroadband OPCPA systems. In the 10-fs FTL case, degradation of the pulse temporal contrast is observed when compensating larger magnitudes of IPR error with tip adjustment. These pulse shapes appear to contain a residual higher-order phase that varies spatially in magnitude and sign, where residual phase cannot be subtracted out by an AOPDF as in Fig. 155.28.

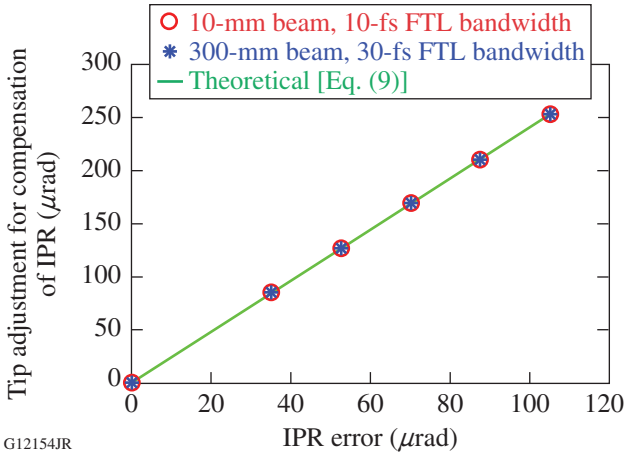

Figure 155.29
Tip angle required to compensate a given IPR error, eliminating first-order vertical angular dispersion. These simulations for two cases of bandwidth and beam size are optimized for shortest pulse duration by adjusting the tip after an IPR error is made on the same grating (markers). Optimized tip adjustments in the simulations are in good agreement with theoretical predictions from Eq. (9) (solid line).

Tip and IPR errors are practically indistinguishable in small amounts when observing the far-field focal spot because they both cause an increase of the spot size in the vertical direction. For small-bandwidth pulses, reducing the observed vertical dispersion in a grating compressor by partial compensation of tip error with IPR, or vice versa, may be acceptable, depending on pulse contrast requirements. In the case of an ultra-broadband pulse, however, this partial compensation may deleteriously affect pulse shape and contrast, as shown in Fig. 155.30(b). In this case, simultaneous monitoring of the pulse duration and contrast would allow proper optimization of the tip and IPR.

Symmetry can be used to relax alignment tolerances if the gratings can be made large enough to hold a second vertically displaced beam. A four-grating compressor can be folded by placing a roof mirror in the plane of symmetry (Fig. 155.21). The roof mirror vertically inverts the beam for a second pass through the same grating pair, where any vertical angular dispersion or vertical path deviations from the first pass are

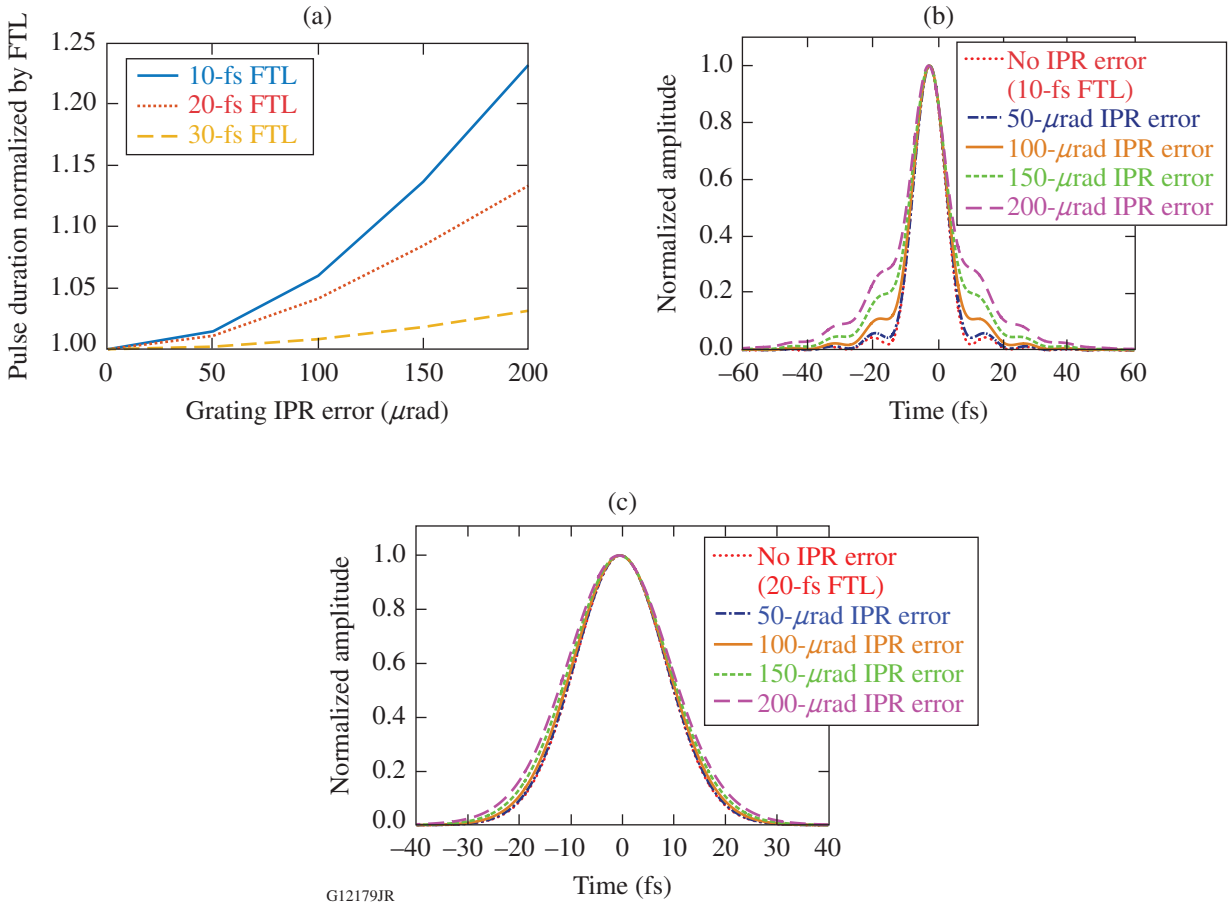

Figure 155.30

(a) Increases in FWHM pulse duration normalized by the FTL are plotted for different magnitudes of IPR error, where angular dispersion has been compensated by a proportional tip adjustment, following Eq. (9). Deformation of pulse shapes are shown for (b) a 10-fs FTL pulse (20th-order super-Gaussian spectrum) and (c) a 20-fs FTL pulse (Gaussian spectrum) for various tip-compensated IPR errors.

reversed and canceled to first order on the second pass. Simulations of tip and IPR error showed that there was no effect on the pulse duration or spot size for errors <1000 μrad, but pulse distortions grew to ~10% for grating errors of 2000 μrad for a 10-fs FTL bandwidth.

Conclusions

In conclusion, the effects of grating-compressor misalignment have been reviewed and simulated in a *FRED–MATLAB* compressor model, showing the alignment sensitivity of tilt, tip, and IPR for a 0.5-PW, 15-fs OPCPA system. These simulations were expanded to estimate grating-tilt–alignment tolerances in a framework of bandwidths ranging from 1000-fs FTL to 10-fs FTL and compressor beam sizes ranging from 10 mm to 300 mm. These tolerances provide guidelines for how compressor alignment sensitivity scales with bandwidth and compressor beam size for mainstream CPA technologies and performance levels. For compressor beam sizes above 100 mm and transform-limited pulse durations below 30 fs, alignment tolerances decrease significantly, and individualized simulation is recommended for more-accurate specification of grating mount precision and stability requirements or for application-specific tolerance definition.

Supplementary scaling of grating-alignment tolerances with all possible combinations of groove density and incident angle was simulated for a 30-fs FTL bandwidth and 100-mm beam size. Compressor geometries where the incident angle was smaller than the diffracted angle were most sensitive to misalignment, as well as compressors at any incident angle with grating groove density >1500 gr/mm.

Sources of compressor alignment error and methods for alignment were discussed. Compensating the residual chirp

that results from grating-tilt error by adjusting the grating separation was shown to partially decrease pulse distortions in simulations. Arbitrary shaping of the spectral phase by using an AOPDF was shown to further decrease the pulse distortion caused by grating-tilt error.

Simulations showing the compensation of IPR error with tip adjustment (and vice versa) were performed for varying bandwidths and beam sizes. Temporal contrast degradation and serious pulse distortion were observed for FTL pulse durations below 20 fs and compensated IPR/tip errors larger than ~200 μrad, with no obvious effect on the focused spot size. A practical optimization method for IPR and tip alignment was discussed.

Alignment can be significantly simplified in a folded compressor comprised of a single grating pair and a vertical roof mirror since vertical components of angular dispersion are canceled to first order. Tip and IPR errors up to 1000 μrad were simulated with no effect on the pulse duration or focused spot size. As a consequence of double passing each grating, the tilt-alignment sensitivity is increased by a factor of 2.

To our knowledge this is the first time compressor alignment tolerances have been simulated over a broad range of bandwidths, compressor beam sizes, incident angles, and grating groove densities and applied generally to all mainstream CPA technologies ito illustrate tolerance scaling. Furthermore, several compressor misalignment compensation strategies were studied in *FRED–MATLAB* to identify bandwidth, temporal contrast, and error-magnitude limitations.

ACKNOWLEDGMENT

This material is based upon work supported by the Department of Energy National Nuclear Security Administration under Award Number DE-NA0001944, the University of Rochester, and the New York State Energy Research and Development Authority. The support of DOE does not constitute an endorsement by DOE of the views expressed in this article.

REFERENCES

1. D. Strickland and G. Mourou, Opt. Commun. **55**, 447 (1985).
2. A. Klenke *et al*., Opt. Lett. **38**, 2283 (2013).
3. Z. Gan *et al*., Opt. Express **25**, 5169 (2017).
4. K. Osvay and I. N. Ross, Opt. Commun. **105**, 271 (1994).
5. Z. Wang, Z. Xu, and Z.-Q. Zhang, IEEE J. Quantum Electron. **37**, 1 (2001).
6. G. Pretzler, A. Kasper, and K. J. Witte, Appl. Phys. B **70**, 1 (2000).
7. K. Osvay *et al*., IEEE J. Sel. Top. Quantum Electron. **10**, 213 (2004).
8. C. Fiorini *et al*., IEEE J. Quantum Electron. **30**, 1662 (1994).
9. O. E. Martinez, J. Opt. Soc. Am. B **3**, 929 (1986).
10. J.-C. Chanteloup *et al*., J. Opt. Soc. Am. B **17**, 151 (2000).
11. *FRED*, Photon Engineering LLC, Tucson, AZ 85711.
12. M. Guardalben and G. Dahl, *EPCOMP*, a beam-propagation code developed at the Laboratory for Laser Energetics, University of Rocheser, Rochester, NY (2004) (unpublished).
13. J. Bromage, presented at The 3rd International Symposium on High Power Laser Science and Engineering, Suzhou, China, 9–13 April 2018.
14. J. Qiao, A. Kalb, M. J. Guardalben, G. King, D. Canning, and J. H. Kelly, Opt. Express **15**, 9562 (2007).
15. The MathWorks Inc., Natick, MA 01760-2098.
16. P. Poole *et al*., Opt. Express **21**, 26,341 (2013).
17. F. Canova *et al*., Opt. Express **15**, 15324 (2007).
18. J. L. Collier *et al*., *Central Laser Facility Annual Report 2002/2003*, 168, Rutherford Appleton Laboratory, Chilton, Didcot, Oxon, England, RAL Report No. RAP-TR-2003-018 (2003).
19. M. J. Guardalben, Appl. Opt. **47**, 4959 (2008).
20. F. Verluise *et al*., Opt. Lett. **25**, 575 (2000).